

Preparation and characterization of Sr-Ti-hardystonite (Sr-Ti-HT) nanocomposite for bone repair application

^{1*}H. Mohammadi; ^{2,3}M. Hafezi; ²S. Hesaraki; ⁴M.M. Sepantafar

¹Department of Biomaterials, Science and Research Branch, Islamic Azad University, Yazd, Iran

²Biomaterials Group, Nanotechnology and Advanced Materials Department, Materials and Energy Research Center, Alborz, Iran

³Pardis Pajooheh Fanavarani Yazd, BT center, Yazd Science and Technology Park, Yazd, Iran

⁴Department of Stem Cell and Developmental Biology at Cell Science Research Center, Royan Institute for Stem Cell Biology and Technology, ACECR, Tehran, Iran

Received: 15 February 2015

Accepted: 20 May 2015

ABSTRACT:

Objective(s): Hardystonite (HT) is Zn-modified silicate bioceramics with promising results for bone tissue regeneration. However, HT possesses no obvious apatite formation. Thus, in this study we incorporated Sr and Ti into HT to prepare Sr-Ti-hardystonite (Sr-Ti-HT) nanocomposite and evaluated its in vitro bioactivity with the purpose of developing a more bioactive bone substitute material.

Materials and methods: The HT and Sr-Ti-HT were prepared by mechanical milling and subsequent heat treatment. Calcium oxide (CaO), zinc oxide (ZnO) and silicon dioxide (SiO₂) (all from Merck) were mixed with molar ratio of 2:1:2. The mixture of powders mixture was then milled in a planetary ball mill for 20 h. In the milling run, the ball-to-powder weight ratio was 10:1 and the rotational speed was 200 rpm. After synthesis of HT, 3% nanotitanium dioxide (TiO₂, Degussa) and 3% strontium carbonate (SrCO₃, Merck) were added to HT and then the mixture was ball milled and calcined at 1150°C for 6 h. Simultaneous thermal analysis (STA), X-ray diffraction (XRD), Transmission electron microscopy (TEM) and Fourier transform infra-red spectroscopy (FT-IR) performed to characterize the powders.

Results: XRD and FT-IR confirmed the crystal phase and silicate structure of HT and TEM images demonstrated the nanostructure of powders. Further, Sr-Ti-HT induced apatite formation and showed a higher human mesenchymal stem cell (hMSCs) adhesion and proliferation compared to HT.

Conclusion: Our study revealed that Sr-Ti-HT with a nanostructured crystal structure of 50 nm, can be prepared by mechanical activation to use as biomaterials for orthopedic applications.

Keywords: Apatite formation, Hardystonite, Mechanical activation, Mesenchymal stem cells, Nanocomposite

INTRODUCTION

During the past three decades, by growing the aging population, bone loss is a progressively serious problem. Autologous bone transplantation was considered as the most effective treatment, however not enough donor tissue and the morbidity have restricted this strategy in large-scale applications. In addition, allogenic or xenogenic bone grafts can cause

immunological reactions in the patients, imposing a key limit on their clinical application. In recent years, silicate bioceramics (CaSiO₃) have introduced as a new class of biomaterials for bone repair applications, however, their major drawbacks are high degradation rate leading to a high environmental pH affecting their osseointegration ability [1, 3] and inability to support human bone proliferation [4]. One way to control dissolution of biomaterials is the incorporation of metals into the CaSiO₃ [5]. There are several metals which have influence on bone formation. Zinc (Zn) is an important inorganic ion for growth and development

*Corresponding Author Email: hosseinmochican@gmail.com
Tel: 0912-7926642

Note. This manuscript was submitted on February 15, 2015; approved on May 20, 2015

of healthy bone which stimulates bone formation and inhibits bone resorption [6,8]. Also, Strontium (Sr), known as bone seeking inorganic ion, supports osteogenesis [9, 10]. Further-more, it has been shown that titanium (Ti) significantly promotes osteoblast proliferation, differentiation and mineralization [11, 12]. By the incorporation of Zn into CaSiO_3 , hardystonite ($\text{Ca}_2\text{ZnSi}_2\text{O}_7$, HT) is formed which indicated a more chemically stable material and showed promising results for bone tissue regeneration [13,15]. The incorporation of Sr into HT ceramic was used to improve the biological performance [16]. However, both HT and Sr-HT possessed no obvious apatite mineralization [16, 17]. Thus, the aim of this is to determine the simultaneous effect of Sr and Ti on the microstructures, apatite formation and biocompatibility of HT as a bone substitute biomaterial.

MATERIALS AND METHODS

Synthesis of powders

The HT powders were prepared by the mechanical activation and heat treatment method using calcium oxide (CaO), zinc oxide (ZnO) and silicon dioxide (SiO_2) as raw materials (all from Merck, Germany). Briefly, CaO, ZnO and SiO_2 were mixed with molar ratio at 2:1:2. The powders mixture was then ball milled for 20 h in a planetary ball mill (Retsch, PM 100) under ambient conditions. The milling media comprised of zirconia vial with ten zirconia balls, 10 mm in diameter. Also, the ball-to-powder weight ratio was 10:1 and the rotational speed was set at 200 rpm. After synthesis of HT, Sr-Ti-HT powders was prepared by adding 3% nanotitanium dioxide (TiO_2 , Degussa) and 3% strontium carbonate (SrCO_3 , Merck) to HT and then the mixture was ball milled as described above and calcined at 1150°C for 6 h.

Powder characterization

Differential thermal analysis (DTA) and Thermal gravimetric analysis (TGA)

The thermal behavior of the initial prepared powder was studied by simultaneously thermal analysis (STA). A thermoanalyzer (Netzsch STA 409 PC/PG) that covers the thermal range between ambient temperature and up to 1200°C with the heating rate of $10^\circ\text{C min}^{-1}$ was used to record the conventional thermoanalytical curves.

X-ray diffraction

The resulting powders were analyzed by X-ray diffraction (XRD) with Philips PW 3710 diffractometer. This instrument was operated with voltage and current settings of 40 kV and 40 mA, respectively and uses $\text{Cu-K}\alpha$ radiation (1.540600 \AA). For qualitative analysis, XRD diagrams were recorded in the interval $10^\circ \leq 2\theta \leq 60^\circ$ at scan speed of 2° min^{-1} representing the step size of 0.02° and the step time of 1s.

Fourier transform infra-red spectroscopy

The powder samples were examined by Fourier transform infra-red (FT-IR) with Thermo Nicolet spectrometer. For IR analysis, at first 1 mg of the powder samples were carefully mixed with 300 mg of KBr (infrared grade) and palletized under vacuum. Then the pellet was analyzed in the range of 400 to 4000 cm^{-1} at the scan speed of 23 scan min^{-1} and the resolution of 4 cm^{-1} .

Transmission electron microscopy

The final synthesized powder was observed by transmission electron microscopy (TEM, GM200 PEG Philips, Netherlands). For this purpose, the particles were deposited onto Cu grids, which support a carbon film by deposition from a dilute suspension in ethanol.

Scanning electron microscopy

The samples were coated with a thin layer of Gold (Au) by sputtering (EMITECH K450X, England) and then the microstructure of the sample was observed on a scanning electron microscope (SEM; Philips XL 30).

Bioactivity test and chemical stability

To assess the bioactivity of powders, simulated body fluids (SBF) containing ion concentrations similar to those in human blood, was prepared as described by Kokubo [18] (Table.1). Briefly, reagent -grade CaCl_2 , $\text{K}_2\text{HPO}_4 \cdot 3\text{H}_2\text{O}$, NaCl, KCl, $\text{MgCl}_2 \cdot 6\text{H}_2\text{O}$, NaHCO_3 , and Na_2SO_4 were dissolved in distilled water and pH was adjusted to 7.4. HT and Sr-Ti-HT powders were incubated in SBF at 37°C for 1, 3, 7, 14 and 28 days, and the ratio of powder surface area to solution volume of SBF was $0.1 \text{ cm}^2/\text{mL}$ [19]. The pH value of the solution was continually monitored for 28 days using an electrode-type pH meter (EcoMet P25, Istek, South Korea). At 5 days of soaking, the Sr-Ti-HT powders were analyzed by XRD and SEM. The XRD diagrams

were recorded in the interval 20° d' 2è d' 40° at scan speed of 2° min⁻¹ representing the step size of 0.02° and the step time of 1s.

Cell viability assay

It is widely agreed that in vitro testing of processes are of great importance in cytotoxicity investigations of a biomaterial [20, 21]. According to International standard (ISO-10993-5), MTT assay can be used in this evaluation. Briefly, HT and Sr-Ti-HT were separately grounded and sieved; the size varies (100-600 μm). The two samples were sterilized under dry heat at 180°C. Under sterile environments, samples were immersed in the culture medium in a humidified atmosphere of 5% CO₂ and 95% air. The ratio of powder weight in (mg) to medium (F-12) volume in (ml) was 200 mg/ml. After incubation for 2, 4, 8, 16, 24, 48 and 72 h, the suspension was centrifuged, and then the supernatant was gathered as extracts. After that, microscopic images of three samples were obtained using inverted microscope (Olympus CKX41, USA). The extractions from similar ones (24, 48 and 72 h) were used for MTT assays. Human mesenchymal stem cells (hMSCs) were harvested and the cell suspension was regulated to a density of 1.0×10⁴ cells cm⁻²; then 100 μl of the cell suspension was added to each well of 96-well-plate. After incubation in 37°C for 24 h, the culture medium was removed and substituted by 50 μl of extract and 50 μl F-12 of medium supplemented with 10% FBS. Cells were cultured in vitro with extracts and after incubation in 95% air humidity and 5% CO₂ at 37°C for 1, 3 and 7 days, respectively, the 3-(4,5-dimethylthiazol-2-yl)-2,5-diphenyl tetrazolium bromide (MTT) solution was added to each well (100 μl per well of a 0.5 mgml⁻¹ MTT solution in PBS) and incubated for 4 h at 37°C. The supernatant was removed and insoluble formazan crystals were dissolved in 100 μl dimethylsulfoxide (DMSO) in each well. The optical density (OD) was measured at 570 nm using a microplate reader (EL×800, BIO-TEK). For the MTT experiment, two groups (HT-24, HT-72) and (Sr-Ti-HT-24, Sr-Ti-HT-72) were tested: complete liquid culture medium as negative or non-toxic control, at various time periods (1, 3 and 7 days). Two independent experiments were performed with three samples per group (n=3). Mean values±standard deviation (SD) of absorbance values acquired from cells incubated in the presence of extracts, either from controls or material extracts, were calculated. Results, for MTT assay, were expressed as

the percentage of the corresponding negative control conducted in similar experiment. Statistical analysis was done through analysis of variance (ANOVA) to evaluate the different cell viability. A p*-value <0.05 was deliberated statistically significant.

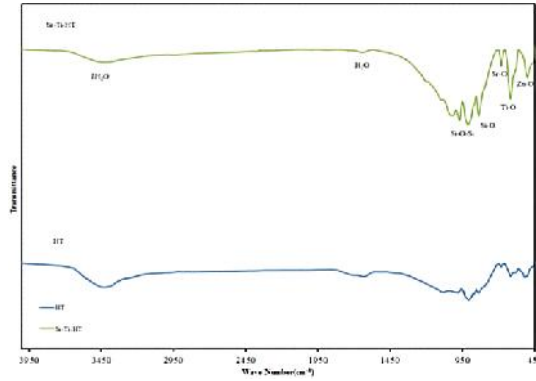


Fig. 1. STA curve of initially mechanically activated powders for 20 h

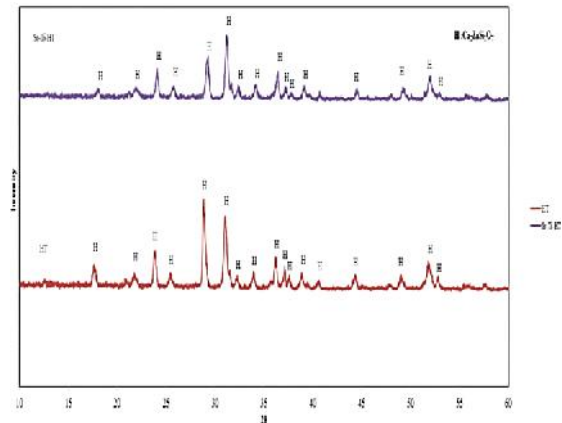


Fig. 2. XRD patterns of mechanically activated powders after heat treatment at 1150 °C for 6 h

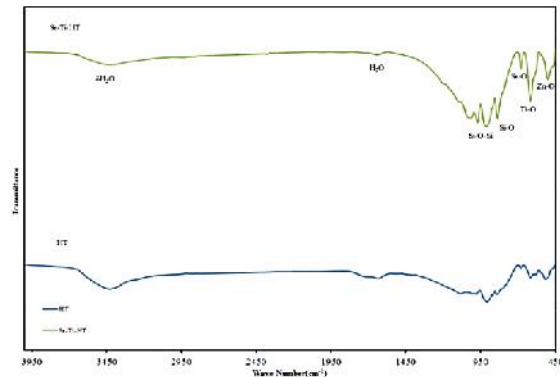


Fig. 3. FTIR spectra of mechanically activated powders after heat treatment at 1150 °C for 6 h

Table 1. Ion concentration of SBFs and human blood plasma (mM)

	Na ⁺	Mg ²⁺	K ⁺	Ca ²⁺	Cl ⁻	HCO ₃ ⁻	HPO ₄ ²⁻	SO ₄ ²⁻
Human blood plasma	142.0	1.5	5.0	2.5	103.0	27.0	1.0	0.5
Original SBF	142.0	1.5	5.0	2.5	148.8	4.2	1.0	0.0

RESULTS

Characterization of HT

According to the simultaneous thermal analysis (Fig. 1), differential thermal analysis (DTA) curve, showed an endothermic peak around 400 °C which is attributed to elimination of water molecule and organic phases. Then, one weak exothermic peak was observed at 650 °C that can be possibly due to the mathematical sum of and exothermic decomposition [22] After that, the main exothermic peak was found at 850 °C which is related to the crystallization temperature of HT [23]. An endothermic peak at 1180 °C is attributed to the melting point of HT. The thermogravimetric analysis (TGA) curve showed three main stages for weight loss. At first, adsorbed water molecules were eliminated in heating up to 370 °C [24]. Then, 7% weight loss was observed between 370-420 °C due to elimination of organic phases and finally nearly 5% till the end of procedure. According to XRD pattern (Fig 2), after heat treatment at 1150 °C, the pattern was belonged to HT phase (Standard cards JCPD No. 00-035-0745) [14]. As shown in FTIR spectra (Fig. 3) the intense bands at around 1667 and 3456 cm⁻¹ related to the bending and stretching vibrational water due to the exposure of powders to atmosphere [25]. Further, the band at 840 cm⁻¹ is attributed to Si-O bond [26], the band at 973 and 918 cm⁻¹ was assigned to asymmetric stretching vibration of Si-O-Si bond [27, 28].

Characterization of Sr-T-HT

As it was observed in XRD pattern (Fig. 2), the pattern was belonged to HT phase (Standard cards JCPD 00-035-0745) [14]. Further, a slight deviation (shift to the right) was observed. The crystallite size of Sr-Ti-HT was obtained 41 nm by the Williamson-Hall equation (eq.1) [29]:

$$\Delta \cos \theta = K\lambda / D + 2A \sin \theta \quad (1)$$

in which, K is a dimensionless shape factor of the crystallite (expected value is 0.94), λ is the wavelength, $\Delta \cos \theta$ is the line broadening at full width at half maximum (FWHM), D is average crystallite size, ϵ is average residual strain in powder, θ is the Bragg angle and A is coefficient which depends on strain distribution. The FT-IR spectra (Fig. 3) showed that the intense bands at around 1667 and 3456 cm⁻¹ related to the bending and stretching vibrational water due to the exposure of powders to atmosphere [25]. Also, the band at 840 cm⁻¹ is attributed to Si-O bond [26], the band at 973 and 918 cm⁻¹ was assigned to asymmetric stretching vibration of Si-O-Si bond [27, 28]. There are several peaks in the range of 500-1000 cm⁻¹ which are typically related to the absorption of metal-oxygen [30]. The band at 503 cm⁻¹ is associated with Zn-O bond [31], the band at 620 cm⁻¹ is related to Ti-O(26, 32) and the band at 682 cm⁻¹ may be possibly associated with Sr-O stretching frequency. As it is observed in TEM image (Fig. 4), the nanostructure of composite was demonstrated, in which the grain size was nearly 50 nm as well as the rounded shape crystallite size.

Bioactivity test and chemical stability

The changes in pH values of the SBF solution for 28 days (Fig. 5) stated that the pH values of Sr-Ti-HT and HT were considerably reduced compared to that of previously reported for CaSiO₃ [33]. Both of them induced a quick increase of pH value in the first 24 h of soaking which can be attributed to the formation of a hydrated silica layer on the surface [34]. However, for Sr-Ti-HT, the increase of pH was reached to 8 compared to that of 10 for HT. According to XRD pattern of Sr-Ti-HT powders (Fig. 6) after soaking for 5 days, apatite layer deposition was induced on the surface (Standard cards JCPD No. 00-024-0033) (14, 35) which is confirmed by SEM image (Fig. 7), whereas, this was not observed for HT.

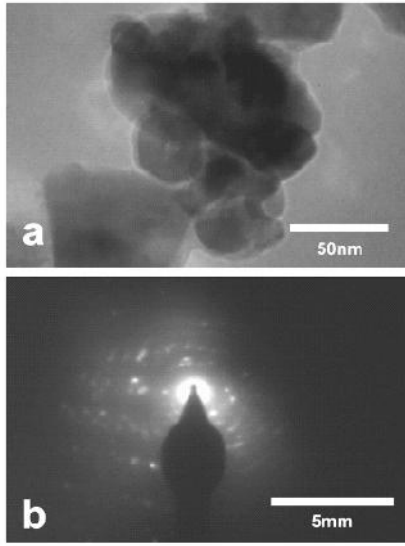


Fig. 4. TEM micrograph of mechanically activated Sr-Ti-HT powder after heat treatment at 1150 °C for 6 h

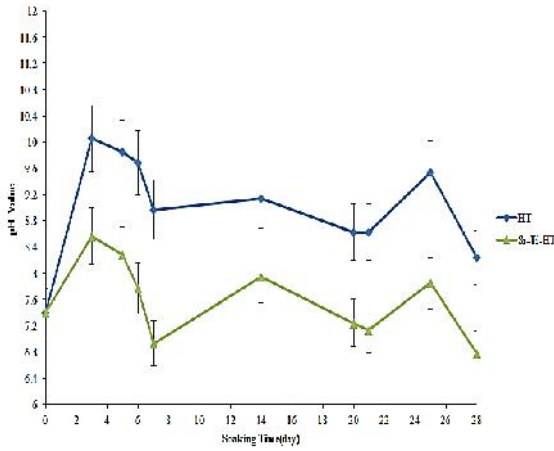


Fig. 5. The change of pH value HT and Sr-Ti-HT powders after soaking in SBF for 28 days

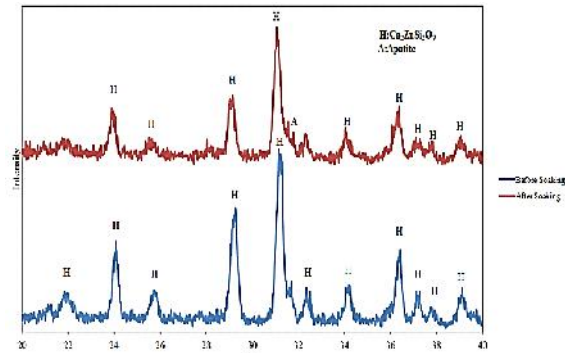


Fig. 6. XRD pattern of Sr-Ti-HT powders after soaking in SBF for 5 days

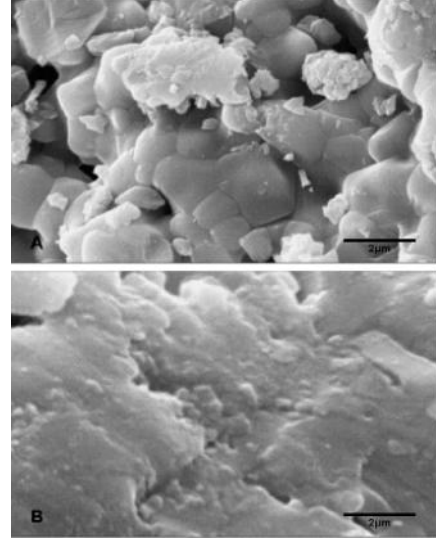


Fig. 7. SEM micrograph of (A) Sr-Ti-HT and (B) HT powders after soaking in SBF for 5 days

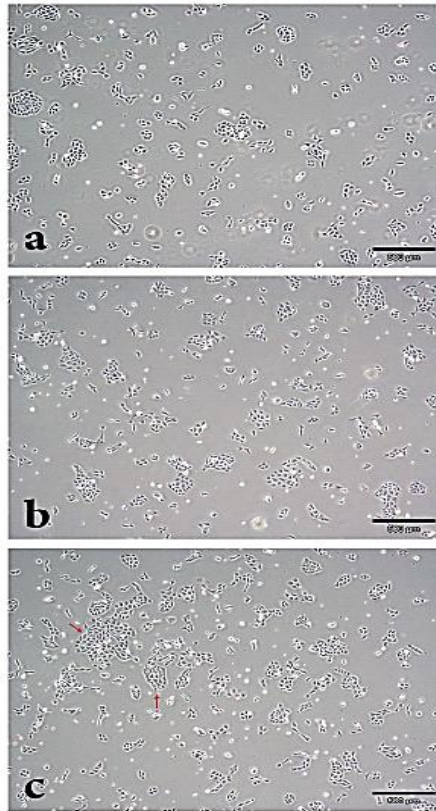


Fig. 8. Light micrographs of cell distribution (a) control (b) HT and (c) Sr-Ti-HT powders

Cell culture and viability assay

The hMSCs viability and proliferation were evaluated by MTT assay. The cell proliferation in Sr-Ti-HT extract was considerably different from that of HT and control sample. According to light microscopic images of the three samples after 48 h (Fig 8), there were no obvious difference between samples, but after 72 h, a distinct cell distribution was observed, in which the Sr-Ti-HT showed significantly higher cell proliferation than HT and control sample (red arrows). The density of the cells improved by the extension of the culture time and this indicated the higher cell proliferation at 7 days. The hMSCs cultured on Sr-Ti-HT showed a significantly ($p < 0.05$) higher proliferation rate at 1, 3, and 7 days of culture compared to that of HT and control sample and gradually increased during the culture period due to the chemical stability and different chemical composition (Fig 9).

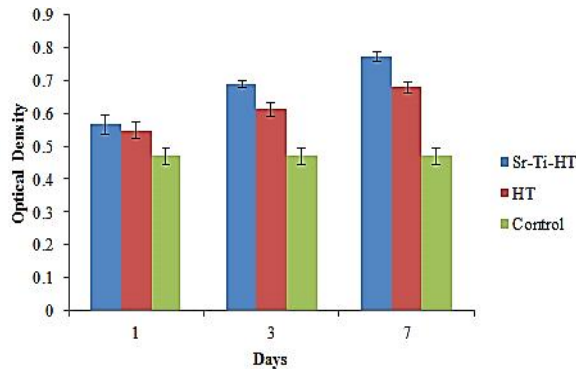
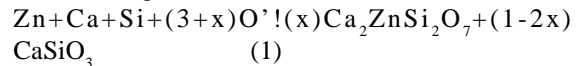


Fig. 9. Human mesenchymal stem cells proliferation on control, HT and Sr-Ti-HT powders at 1,3 and 7 days of culture p value < 0.05

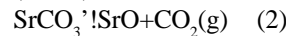
DISCUSSION

In this study, we have successfully prepared Sr-Ti-HT and HT powders through mechanical activation and heat treatment. The DTA-TGA analysis showed that the HT phase was formed in 850°C as indicated by exothermic peak. The XRD data showed that only HT crystal phase was appeared. Also, the observed slight deviation in XRD pattern of Sr-Ti-HT is probably due to the larger ionic radii of Sr and Ti. In addition, the peak intensity of Sr-Ti-HT was decreased probably due to the structural strain of Sr [36, 37]. The FTIR spectra revealed that the silicate structure did not change in both HT and Sr-Ti-HT powders and no carbonate phase was observed. As it can be seen in TEM image, Sr-Ti-HT revealed a nearly agglomerative morphology with rounded shape. However, the they were not stable. Previous studies have

shown that chemical stability can affect the cascade of cellular and molecular events [14, 19]. The pH value of SBF solution for the resultant Sr-Ti-HT and HT powders revealed a lower dissolution rate in SBF compared to that of previously reported for CaSiO_3 [33]. This indicated their improved chemical stability as well as the role of metals in controlling the dissolution rate of biomaterials [38]. Zn ion can react with calcium, Si and O to form a new crystal phase of HT [13]. It is suggested that in the Zn-Ca-Si system, the following reaction is occurred as follows [14]:



Further, SrCO_3 is decomposed to SrO and CO_2 at high temperatures, according to the reaction as follows (39, 40):



However, it may be elucidated that the Sr-Ti-HT powder increased pH in the first day of soaking up to 8 compared to that of 10 for HT. The bone bonding capability of materials is often assessed through investigating the ability of apatite formation on the surface in a SBF solution [18]. Bioactive materials have the ability to bond with the living bone tissue through the formation of a biological apatite layer on their surface both in vitro and in vivo [13, 41]. The dissolution of HT is very slow and has no obvious apatite formation as previously reported [14, 17, 42]. Furthermore, previous studies have shown that the presence of Ti and Sr induce apatite nucleation [43, 44]. In this study, Sr-Ti-HT induced apatite formation after 5 days of soaking in SBF while, this was not observed for HT (see Fig.7). Human mesenchymal stem cells (hMSCs) are attractive cell source for tissue regeneration because they possess high degree of proliferation and the ability to differentiate into different lineages-like osteoblasts cells (45, 46). The biocompatibility of Sr-Ti-HT and HT powder was evaluated by determining the adhesion and proliferation of hMSCs on the powders. Overall, HT and Sr-Ti-HT showed good biocompatibility. However, Sr-Ti-HT revealed a higher hMSCs cell proliferation compared to HT. The chemistry of materials and their composition has a great influence on the cell behaviour. Sr, Ti and Zn have been shown to be very beneficial to the growth and proliferation of bone-related cells [11, 47, 48]. Thus, it is speculated that the incorporation of Sr and Ti into the HT, improved the bioactivity which may result in a more

bioactive material for bone tissue engineering. However the mechanical properties and further in vivo study are needed to be evaluated.

CONCLUSION

The Sr-Ti-HT nanocomposite was prepared by mechanical activation and heat treatment. Simultaneously incorporation of Sr and Ti improved the chemical stability and bioactivity of HT. It induced apatite formation on the surface and further supported higher hMSCs cell proliferation rate compared to HT. All the results postulated that Sr-Ti-HT might be regarded as bone regenerative material.

ACKNOWLEDGEMENTS

This study supported by Pardis Pajooohesh Fanavarn Yazd Company and Biotechnology Center of Yazd Science and Technology Park (YSTP). The authors would like to thank for their supports. The authors also declare no conflict of interests.

REFERENCES

1. De Aza PN, Fernández-Pradas JM, Serra P. In vitro bioactivity of laser ablation pseudowollastonite coating. *Biomaterials*. 2004; 25(11): 1983-90.
2. El-Ghannam A, Ducheyne P, Shapiro IM. Porous bioactive glass and hydroxyapatite ceramic affect bone cell function in vitro along different time lines. *J Biomed Mater Res*. 1997; 36(2): 167-80.
3. Xue W, Liu X, Zheng X, Ding C. In vivo evaluation of plasma-sprayed wollastonite coating. *Biomaterials*. 2005; 26(17): 3455-60.
4. Wu C. Methods of improving mechanical and biomedical properties of Ca-Si-based ceramics and scaffolds. *Expert Rev Med Devices*. 2009; 6(3): 237-41.
5. Mohammadi H, Hafezi M, Nezafati N, Heasarki S, Nadernezhad A, Ghazanfari SMH, et al. Bioinorganics in Bioactive Calcium Silicate Ceramics for Bone Tissue Repair: Bioactivity and Biological Properties. *J Cera Sci Technol*. 2013; 5(1): 1-12.
6. Yamaguchi M, Ehara Y. Zinc decrease and bone metabolism in the femoral-metaphyseal tissues of rats with skeletal unloading. *Calcif Tissue Int*. 1995; 57(3): 218-23.
7. Yamaguchi M, Inamoto K, Suketa Y. Effect of essential trace metals on bone metabolism in weanling rats: comparison with zinc and other metals' actions. *Res Exp Med*. 1986; 186(5): 337-42.
8. Yamaguchi M, Oishi H, Suketa Y. Zinc stimulation of bone protein synthesis in tissue culture: Activation of aminoacyl-tRNA synthetase. *Biochem Pharmacol*. 1988; 37(21): 4075-80.
9. Capuccini C, Torricelli P, Sima F, Boanini E, Ristoscu C, Bracci B, et al. Strontium-substituted hydroxyapatite coatings synthesized by pulsed-laser deposition: In vitro osteoblast and osteoclast response. *Acta Biomater*. 2008; 4(6): 1885-93.
10. Fredholm YC, Karpukhina N, Law RV, Hill RG. Strontium containing bioactive glasses: Glass structure and physical properties. *J Non-Cryst Solids*. 2010; 356(44-49): 2546-51.
11. Harle J, Kim HW, Mordan N, Knowles JC, Salih V. Initial responses of human osteoblasts to sol-gel modified titanium with hydroxyapatite and titania composition. *Acta Biomater*. 2006; 2(5): 547-56.
12. Vrouwenvelder WC, Groot CG, de Groot K. Better histology and biochemistry for osteoblasts cultured on titanium-doped bioactive glass: bioglass 45S5 compared with iron-, titanium-, fluorine- and boron-containing bioactive glasses. *Biomaterials*. 1994; 15(2): 97-106.
13. Wu C, Chang J, Zhai W. A novel hardystonite bioceramic: preparation and characteristics. *Ceram Int*. 2005; 31(1): 27-31.
14. Wu C, Ramaswamy Y, Chang J, Woods J, Chen Y, Zreiqat H. The effect of Zn contents on phase composition, chemical stability and cellular bioactivity in Zn-Ca-Si system ceramics. *J Biomed Mater Res B Appl Biomater*. 2008; 87(2): 346-53.
15. Zreiqat H, Ramaswamy Y, Wu C, Paschalidis A, Lu Z, James B, et al. The incorporation of strontium and zinc into a calcium-silicon ceramic for bone tissue engineering. *Biomaterials*. 2010; 31(12): 3175-84.
16. Zhang M, Lin K, Chang J. Preparation and characterization of Sr-hardystonite ($\text{Sr}_2\text{ZnSi}_2\text{O}_7$) for bone repair applications. *Mater Sci Eng C*. 2012; 32(2): 184-8.
17. Wu C, Chang J, Xiao Y. Advanced bioactive inorganic materials for bone regeneration and drug delivery: CRC Press; 2013.
18. Kokubo T, Takadama H. How useful is SBF in predicting in vivo bone bioactivity? *Biomaterials*. 2006; 27(15): 2907-15.
19. Wu C, Ramaswamy Y, Soeparto A, Zreiqat H. Incorporation of titanium into calcium silicate improved their chemical stability and biological properties. *J Biomed Mater Res A*. 2008; 86A(2): 402-10.
20. Instrumentation AftAoM. Biological Evaluation of Medical Devices: Tests for Cytotoxicity, in Vitro Methods, ANSI/AAMI/ISO 10993-5:1999: Association for the Advancement of Medical Instrumentation; 1999.
21. Ciapetti G, Cenni E, Pratelli L, Pizzoferrato A. In vitro evaluation of cell/biomaterial interaction by MTT assay. *Biomaterials*. 1993; 14(5): 359-64.
22. Goudouri O, Theodosoglou E, Kontonasaki E, Will J, Chrissafis K, Koidis P, et al. Development of highly porous scaffolds based on bioactive silicates for dental tissue engineering. *Mater Res Bull*. 2014; 49: 399-404.
23. Halliyal A, Hang KW, Haun MJ. Partially crystallizable glass compositions. Google Patents; 1993.
24. Tavangarian F, Emadi R. Mechanism of nanostructure bredigite formation by mechanical activation with thermal treatment. *Mater Lett*. 2011; 65(15-16): 2354-6.
25. Misevicius M, Scit O, Grigoraviciute-Puroniene I, Degutis G, Bogdanoviciene I, Kareiva A. Sol-gel synthesis and investigation of un-doped and Ce-doped strontium aluminates. *Ceram Int*. 2012 ; 38(7): 5915-24.
26. Manso M, Langlet M, Martynez-Duart JM. Testing sol-gel CaTiO_3 coatings for biocompatible applications. *Mater Sci Eng C*. 2003; 23(3): 447-50.
27. Agathopoulos S, Tulyaganov DU, Ventura JMG, Kannan S, Saranti A, Karakassides MA, et al. Structural analysis and

- devitrification of glasses based on the CaO–MgO–SiO₂ system with B₂O₃, Na₂O, CaF₂ and P₂O₅ additives. *J Non Cryst Solids*. 2006; 352(4): 322-8.
28. Zhang W, Shen Y, Pan H, Lin K, Liu X, Darvell BW, et al. Effects of strontium in modified biomaterials. *Acta Biomater*. 2011; 7(2): 800-8.
29. Williamson GK, Hall WH. X-ray line broadening from filed aluminium and wolfram. *Acta Metallurgica*. 1953; 1(1): 22-31.
30. Schrader B. *Infrared and Raman spectroscopy: methods and applications*: John Wiley & Sons; 2008.
31. Kaushik A, Kumar J, Tiwari M, Khan R, Malhotra B, Gupta V, et al. Fabrication and Characterization of Polyaniline–ZnO Hybrid Nanocomposite Thin Films. *J Nanosci Nanotechnol*. 2008; 8(4): 1757-61.
32. Langlet M, Coutier C, Fick J, Audier M, Meffre W, Jacquier B, et al. Sol–gel thin film deposition and characterization of a new optically active compound: Er₂Ti₂O₇. *Opt Mater*. 2001; 16(4): 463-73.
33. Jimori Y, Kameshima Y, Okada K, Hayashi S. Comparative study of apatite formation on CaSiO₃ ceramics in simulated body fluids with different carbonate concentrations. *J Mater Sci Mater Med*. 2005; 16(1): 73-9.
34. Wu C, Chang J, Ni S, Wang J. In vitro bioactivity of akermanite ceramics. *J Biomed Mater Res A*. 2006; 76(1): 73-80.
35. Mishra VK, Srivastava SK, Asthana BP, Kumar D. Structural and Spectroscopic Studies of Hydroxyapatite Nanorods Formed via Microwave Assisted Synthesis Route. *J Am Ceram Soc*. 2012; 95(9): 2709-15.
36. Ardit M, Cruciani G, Dondi M. The crystal structure of Sr-hardystonite, Sr₂ZnSi₂O₇. *Zeitschrift für Kristallographie - Crystalline Materials*. 2010; 225(7): 298-301.
37. Li ZY, Lam WM, Yang C, Xu B, Ni GX, Abbah SA, et al. Chemical composition, crystal size and lattice structural changes after incorporation of strontium into biomimetic apatite. *Biomaterials*. 2007; 28(7): 1452-60.
38. Xiong K, Shi H, Liu J, Shen Z, Li H, Ye J. Control of the Dissolution of Ca and Si Ions from CaSiO₃ Bioceramic via Tailoring Its Surface Structure and Chemical Composition. *J Am Ceram Soc*. 2013; 96(3): 691-6.
39. Arvanitidis I, Sichen D, Seetharaman S, Sohn HY. The intrinsic thermal decomposition kinetics of SrCO₃ by a nonisothermal technique. *Metall and Materi Trans B*. 1997; 28(6): 1063-8.
40. Maitra S, Chakrabarty N, Pramanik J. Decomposition kinetics of alkaline earth carbonates by integral approximation method. *Cerâmica*. 2008; 54(331): 268-72.
41. Hench LL. Biomaterials: a forecast for the future. *Biomaterials*. 1998; 19(16): 1419-23.
42. Wu C, Chang J. A review of bioactive silicate ceramics. *Biomed Mater*. 2013; 8(3): 032001.
43. Li P, Ohtsuki C, Kokubo T, Nakanishi K, Soga N, de Groot K. The role of hydrated silica, titania, and alumina in inducing apatite on implants. *J Biomed Mater Res A*. 1994; 28(1): 7-15.
44. Wu C, Ramaswamy Y, Kwik D, Zreiqat H. The effect of strontium incorporation into CaSiO₃ ceramics on their physical and biological properties. *Biomaterials*. 2007 ; 28(21): 3171-81.
45. Oreffo RC, Cooper C, Mason C, Clements M. Mesenchymal stem cells. *Stem Cell Rev*. 2005; 1(2): 169-78.
46. Mygind T, Stiehler M, Baatrup A, Li H, Zou X, Flyvbjerg A, et al. Mesenchymal stem cell ingrowth and differentiation on coralline hydroxyapatite scaffolds. *Biomaterials*. 2007; 28(6): 1036-47.
47. Marie PJ, Felsenberg D, Brandi ML. How strontium ranelate, via opposite effects on bone resorption and formation, prevents osteoporosis. *Osteoporos Int*. 2011; 22(6): 1659-67.
48. Yamaguchi M. Role of nutritional zinc in the prevention of osteoporosis. *Mol Cell Biochem*. 2010; 338(1-2): 241-54.

How to cite this article:

Mohammadi H, Hafezi M, Hesarak S, Sepantafar MM. Preparation and characterization of Sr-Ti-hardystonite (Sr-Ti-HT) nanocomposite for bone repair application. *Nanomed. J.*, 2015; 2(3): 203-210.